第 30 卷第 5 期 无 机 化 学 学 报 Vol.30 No.5
2014 年 5 月 CHINESE JOURNAL OF INORGANIC CHEMISTRY 1212-1220

Sb 掺杂 $ZnSnO_3$ 透明导电薄膜:制备与性能

储晓菲 贺蕴秋* 李一鸣 黄河洲 刘德宇 陈慧敏 李文有
(同济大学材料科学与工程学院,上海 201800)

摘要:采用溶胶-凝胶法(Sol-Gel)和旋涂法制备了未掺杂的 $ZnSnO_3$ 薄膜和掺入不同物质的量的 Sb 的 $ZnSnO_3$ 薄膜。采用 X 射线衍射(XRD)、场发射扫描电镜(FE-SEM)、X 射线光电子能谱(XPS)、霍尔效应仪(Hall)以及紫外-可见光(UV-Vis)等表征了热处理后薄膜的晶相、微观形貌、晶格缺陷、电学性能以及紫外-可见光透过率。结果表明:所有薄膜都是 $ZnSnO_3$ 结构;与未掺 Sb 的 $ZnSnO_3$ 薄膜相比,掺入 Sb 后的 $ZnSnO_3$ 薄膜的电阻率都有不同程度的降低,其中掺入 8mol%Sb 的薄膜具有最低的电阻率 0.96 Ω·cm;缺陷研究表明:Sb 的掺入使得晶格中的间隙锌离子含量增加,这有利于薄膜电阻率的降低;薄膜的紫外-可见光(UV-Vis)表明:在波长大于 475 nm 的可见光范围内,掺入 Sb 的 $ZnSnO_3$ 薄膜的可见光透过率都在 80%以上。

关键词:导电;透明;薄膜;溶胶-凝胶法
中图分类号:O61 **文献标识码**:A **文章编号**:1001-4861(2014)05-1212-09
DOI:10.11862/CJIC.2014.169

Sb Doped $ZnSnO_3$ Transparent and Conducting Thin Films: Preparation and Property

CHU Xiao-Fei HE Yun-Qiu* LI Yi-Ming HUANG He-Zhou LIU De-Yu CHEN Hui-Min LI Wen-You
(*Department of Materials Science and Engineering, Tongji University, Shanghai*, 201800, *China*)

Abstract: Undoped and Sb doped $ZnSnO_3$ thin films were synthesized by a sol-gel spin-coating method. A comparative study between these films was presented. The structure, electrical and optical properties of $ZnSnO_3$ thin films doped with 0mol%, 1mol%, 8mol% and 30mol% of Sb were investigated by X-ray diffraction (XRD), field emission-scanning electron microscope (FE-SEM), X-ray photoelectron spectroscope (XPS), Hall measurement and ultraviolet-visible spectroscope (UV-Vis). The results show that all films correspond to a pure phase of $ZnSnO_3$ structure and that Sb doped $ZnSnO_3$ films have lower resistivity than those of undoped $ZnSnO_3$ films. The minimum resistivity is obtained in $ZnSnO_3$ films doped with 8.0mol% of Sb. In addition, interstitial zinc ions introduced by antimony ion doping in $ZnSnO_3$ crystal lattice lead to a better conductivity. Furthermore, all doped $ZnSnO_3$ films are with >80% transmittance in the region above 475 nm.

Key words: conducting; transparent; films; sol-gel

0 Introduction

Transparent and conducting oxide (TCOs) thin films have been widely used in flat-panel devices, photovoltaic devices, light emitting diode and other electrode applications due to their high conductivity and high transparence in the visible region[1-4]. TCOs such as indium tin oxide (ITO)[5-6], tin fluorine oxide (FTO)[7] and zinc aluminium oxide (AZO)[8] have been widely used recently. However, one oxide cannot meet different application demands due to its specific characteristics. For example, ITO is the most qualified

收稿日期:2013-11-18。收修改稿日期:2014-02-17。
国家自然科学基金(No.51175162)资助项目。
*通讯联系人。E-mail:heyunqiu@tongji.edu.cn,Tel:021-69580293

transparent electrodes in flat-panel devices because it possesses low resistivity, easy etching and smooth surface. However, in view of low cost and chemical stability in the markets of glass building, FTO films are regarded as a more suitable candidate to replace ITO. Therefore, different systems, namely, ternary oxides as Cd-Sn-O[9], Zn-In-O[10], Zn-Ga-O[11], Zn-Sn-O[9,12-16], Ga-In-O[17] and polycomponent oxides such as Cd-Sb-In-O[18]、Zn-In-Ga-O[19]、Zn-Sn-In-O[20] have been studied in order to achieve various properties. Among these systems, Zn-Sn-O system draws more attention due to the abundant and inexpensive raw materials.

Zn_2SnO_4 and $ZnSnO_3$ have been reported as two phases of Zn-Sn-O system. Several studies have been conducted to investigate the electrical properties and conductive mechanisms of Zn_2SnO_4 films[12,14-15] while there have been few studies on $ZnSnO_3$ films to the best of our knowledge. One study predicts that $ZnSnO_3$ film has a lower resistivity than Zn_2SnO_4 film[21]. In addition, $ZnSnO_3$ has a higher work function (5.3 eV) than that of ITO (4.7 eV) according to Minami et al.[22]. Therefore, $ZnSnO_3$ is considered as an attractive material for p-n type solar cells.

Until now, synthetic method as magnetron sputtering has been developed for fabricating $ZnSnO_3$ thin films[23]. However, $ZnSnO_3$ often coexists with other crystals as ZnO, SnO_2 and Zn_2SnO_4 in the deposited films and the study of conductive mechanisms of $ZnSnO_3$ films is difficult. Besides, other synthetic methods have been used to produce pure $ZnSnO_3$ micro- and nanostructures. For example, polycrystalline $ZnSnO_3$ powders have been synthesized by a solid-state reaction under high pressure (7 GPa) at elevated temperature (1 000 ℃) and first-principles study of structure properties of $ZnSnO_3$ has been reported[24]. And $ZnSnO_3$ nanowires have been synthesized by thermal evaporation of ZnO, SnO_2 and graphite mixture powders and gas sensing properties of $ZnSnO_3$ nanowires have been studied[25]. In the work of He et al[26], pure transparent and conductive $ZnSnO_3$ thin films were obtained by a sol-gel method. However, the resistivity of pure $ZnSnO_3$ films critically limits the practical applications. Based on the work of He et al, Sb^{3+} and Sb^{5+} ion doped $ZnSnO_3$ was further studied to improve the conductivity.

The mechanism of electrical conductance for $ZnSnO_3$ can be attributed to the existence of localized Zn^{2+} and Sn^{4+} in the $ZnSnO_3$ lattice. By doping of antimony ion n-type conductivity of $ZnSnO_3$ thin films can be improved efficiently because of the introduction of Sb^{3+} ions and Sb^{5+} ions. Zn^{2+} and Sn^{4+} ions have electronic configuration of $(n-1)d^{10}ns^0$(n=4, 5)[27]. Sb^{3+} and Sb^{5+} ions have similar $4d^{10}5s^2$ and $4d^{10}$ electronic configurations, respectively[28]. And Sb^{3+} ion (0.076 nm) and Sb^{5+} ion (0.060 nm) have similar radius to that of Zn^{2+} ion (0.090 nm) and Sn^{4+} ion (0.069 nm). So Sb^{3+} ions and Sb^{5+} ions may replace Zn^{2+} ions or Sn^{4+} ions and generate more interstitial ions than other common dopants for $ZnSnO_3$ films.

Therefore, Sb doped $ZnSnO_3$ thin films were fabricated on quartz substrates by a sol-gel spin-coating method. The effects of antimony ion doping on the crystal structure, surface morphology, chemical states of elements, resistivity, and mobility of $ZnSnO_3$ films were investigated.

1 Experimental

The undoped and Sb doped $ZnSnO_3$ films with a thickness of about 100 nm were prepared by using a sol-gel process in combination with the spin-coating method. Zinc acetate dehydrate ($Zn(Ac)_2\cdot 2H_2O$) and tin chloride pentahydrate ($SnCl_4\cdot 5H_2O$) were used as precursors for $ZnSnO_3$ films. Antimony trichloride ($SbCl_3$) was added to introduce Sb dopant. Ethylene glycol monomethyl ether ($HOCH_2CH_2OCH_3$) was used as solvent. Monoethanolamine ($HOCH_2CH_2NH_2$, MEA) was used as stabilizer to prevent precipitation of the solution. All reagents are analytically pure and bought from Sinopharm Chemical Reagent Co., Ltd..

The concentration of total cations in the solution was 0.4 $mol\cdot L^{-1}$, and MEA to total cations in molar ratio was kept at 0.9. Firstly, a certain amount of $Zn(Ac)_2\cdot 2H_2O$ was dissolved in 82 mL $HOCH_2CH_2OCH_3$. White suspension appeared in 30 min of magnetic stirring. Then $Zn(Ac)_2\cdot 2H_2O$ dissolved when MEA was added into the suspension. The solution kept clear

and stable. Afterward $SnCl_4 \cdot 5H_2O$ was added into $Zn(Ac)_2 \cdot 2H_2O$ solution to get a mixed solution with the molar ratio of Zn to Sn at 1:1. $SbCl_3$ was mixed into the above mixed solution with various $n_{Sb}/(n_{Zn}+n_{Sn})$ molar ratios(1mol%, 8mol% and 30mol%). Finally, the solutions were stirred in a three-neck flask with a flux for 4 h at 80 ℃. The sol solutions were aged in beakers covered with plastic wraps at room temperature for gelation. Before film forming, the colloidal gel suspensions remained clear and fluid. Then they were spin-coated on cleaned quartz glass substrates at a speed of 1 000 r·min^{-1} for 30 s. After spin-coating, films were baked at 300 ℃ for 10 min. The sequence of coating, drying and coating again was performed 3 times. Finally, the films were heat-treated in air at 1 000 ℃ for 6 h with a ramp of 3 ℃·min^{-1}.

The crystalline phases of films with different contents of Sb were identified with the X-ray powder diffraction pattern (XRD:D/max-rB 12 kW, V=40 kV, I =60 mA, Cu $K\alpha$, λ =0.154 18 nm, graphite monochromator, scintillation counter). The surface morphology was examined by field emission scanning electron microscopy (SEM: Quanta 200FEG, HV=20.0 kV). The surface analysis was investigated by X-ray photoelectron spectrometer (XPS: PHI-5000C ESCA System). The free carrier concentration and free carrier mobility were carried out by Hall measurements setup in van der Pauw configuration. The transmittance was obtained by ultraviolet spectrophotometer (UV-Vis: UV-22501PC).

2 Results and discussion

2.1 Structural and morphological studies of $ZnSnO_3$ films

The XRD patterns for films of n_{ZnO}:n_{SnO_2}=1:1 with different doping levels of Sb are shown in Fig.1. It matches with the standard PDF No.28-1486 of phase $ZnSnO_3$. There are no other clear sharp peaks coincident with ZnO, SnO_2, or Zn_2SnO_4. The introduction of Sb does not change the crystal structure of Sb doped $ZnSnO_3$ films and some kinds of $ZnSnO_3$ solid solutions with different crystal defects could be formed through the substitution of Zn or Sn

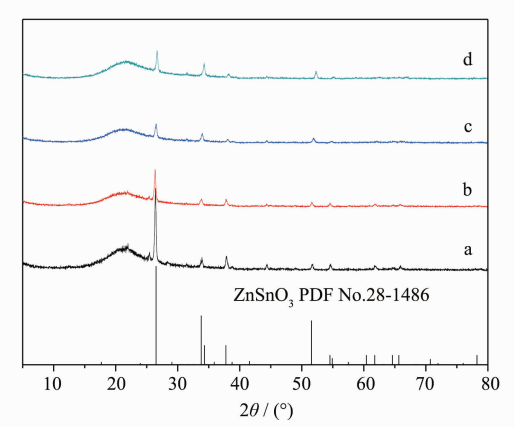

(a) 0mol%, (b) 1mol%, (c) 8mol%, (d) 30mol%

Fig1 XRD patterns for films of composition ZnO:SnO_2= 1:1 with different doping levels of Sb

by Sb. However, with increasing antimony ion doping, the intensity and sharpness of diffraction peaks decrease, indicating that the crystallinity is damaged by the presence of Sb in $ZnSnO_3$ crystal structure. Antimony generally exists as Sb^{5+} and Sb^{3+} in solid solutions. Possible substitution of Zn^{2+} and Sn^{4+} by Sb^{3+} or Sb^{5+} forms impurity defects and disturbs local ordering of the crystal structure, thus leading to lower diffraction intensity and less sharpness of the diffraction peaks.

The SEM images of the $ZnSnO_3$:Sb are shown in Fig.2 (a) ~(c). The surface morphology undergoes substantial changes with increasing doping of Sb. Voids are observed on the surface of $ZnSnO_3$:Sb film synthesized with 1mol% ratio of Sb. As molar ratio of Sb increases, the size of voids decreases and the surface of the $ZnSnO_3$:Sb films becomes relatively smooth.

2.2 Chemical binding states of $ZnSnO_3$ films

Precise analysis of Sb3$d_{3/2}$ spectra performed on films with 1mol%, 8mol% and 30mol% of Sb are shown in Fig.3(a)~(c). For XPS analysis, no attempt was made to sputtering clean the samples in order to avoid sputter-induced chemical changes on the surface. The Sb3$d_{3/2}$ spectra is divided into two Gaussian lines, one centered at (539.20±0.3) eV(Sb^{3+}) and the other centers at (540.10±0.3) eV(Sb^{5+})[26].The fitted results are also shown in Table 1. In films with 1mol% of Sb, 84.8% of Sb detected is in a

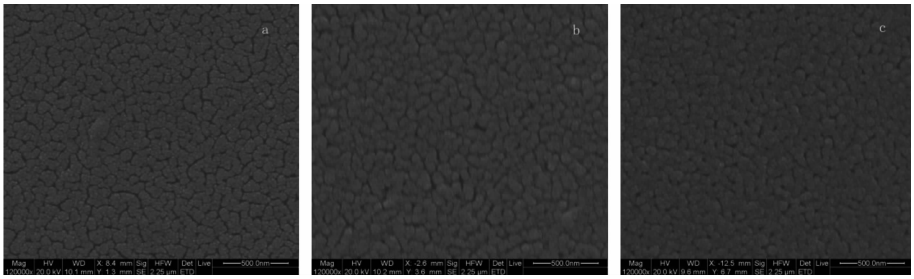

(a) 1mol%, (b) 8mol%, (c) 30mol%

Fig.2　SEM micrograph of $ZnSnO_3$ films with different doping levels of Sb

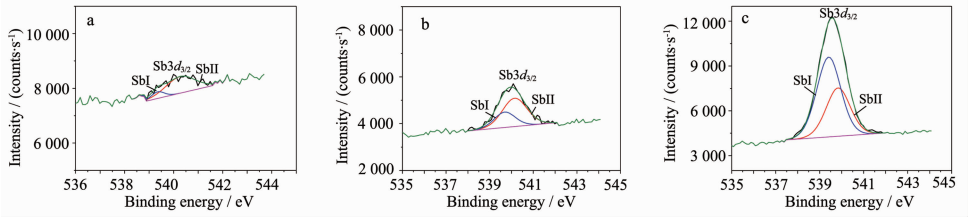

(a) 1mol%, (b) 8mol%, (c) 30mol%

Fig.3　Binding energy of Sb3$d_{3/2}$ in $ZnSnO_3$ films with different doping levels of Sb

Table 1　Binding energy of Sb3d$_{3/2}$ and percentages of antimony in different chemical states in $ZnSnO_3$ films with different doping levels of Sb

Doping concentration / mol%	Sb Ⅰ (Sb^{3+})		Sb Ⅱ (Sb^{5+})	
	Peak / eV	Content / %	Peak / eV	Content / %
1	539.3	15.2	540.3	84.8
8	539.5	32.0	540.1	68.0
30	539.4	62.3	540.0	37.7

pentavalent state (Sb^{5+}) while the other 15.2% is in a tervalent state (Sb^{3+}). As Sb increases to 8mol%, 68.0% of Sb is in a pentavalent state (Sb^{5+}) while the other 32.0% is in a tervalent state (Sb^{3+}). And when Sb finally reaches 30mol%, the percentages of Sb^{5+} decrease to 37.7% while the percentages of Sb^{3+} increase to 62.3%. The percentages of Sb^{3+} gradually increase and finally surpass that of Sb^{5+}. According to XRD analysis, no new phase is formed in Sb doped $ZnSnO_3$ films because antimony atoms totally dissolve in the crystal structure. Therefore, chemical states of Zn, Sn and O could be influenced by substitution of Zn^{2+} and Sn^{4+} by Sb ions in $ZnSnO_3$ solid solutions.

Sn3d spectra of $ZnSnO_3$ films without doping Sb and with 1mol%, 8mol% and 30mol% of Sb are shown in Fig.4(a)~(d). The Sn3$d_{5/2}$ spectra and Sn3$d_{3/2}$ spectra are both divided into two Gaussian lines. The binding energy of Sn3$d_{5/2}$ peaks is centered at (494.80±0.3) eV (Sn Ⅰ) and (495.60±0.3) eV (Sn Ⅱ). The binding energy of Sn3$d_{3/2}$ peaks is centered at (494.80±0.3) eV (Sn Ⅰ) and (495.60±0.3) eV(Sn Ⅱ). Sn Ⅰ and Sn Ⅱ are attributed to Sn in $ZnSnO_3$ crystal lattice and to Sn adjacent to lattice oxygen vacancy, respectively[12]. The chemical states of Sn in $ZnSnO_3$ films with different doping levels of Sb are shown in Table 2 based on XPS analysis (Fig.4). As shown in Table 2, all Sn ions are at original lattice site in undoped $ZnSnO_3$ films. For films with 1mol% of antimony ion doping, Sn ions of original lattice site decrease to 66.0% while tin adjacent to lattice oxygen vacancy increases to 34.0%. When antimony ion doping increases to 8mol%, Sn at original sites increases to 85.0% and Sn adjacent to oxygen vacancy decreases to 15.0%. When with 30mol% of Sb, again Sn ions are all at original lattice

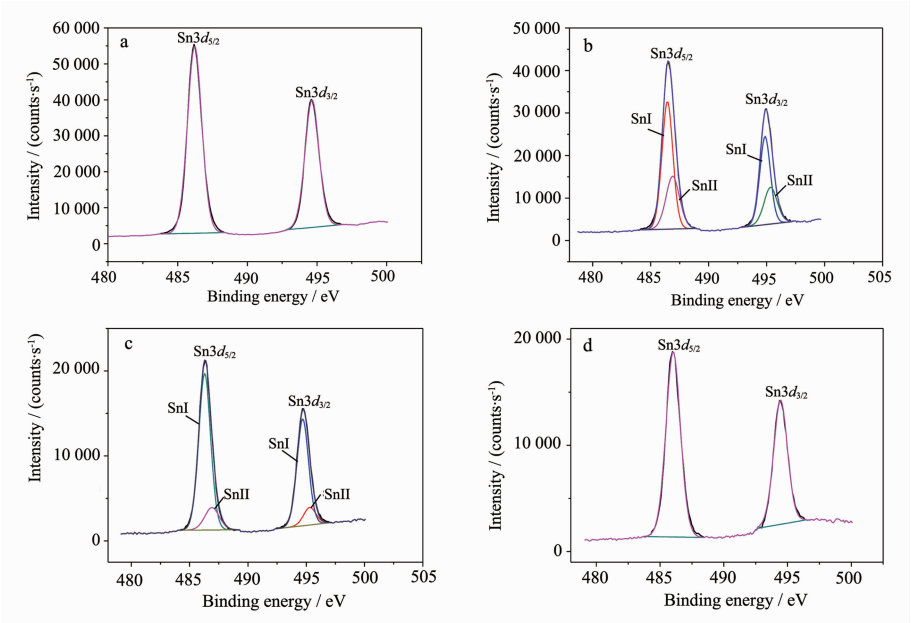

(a) 0mol%, (b) 1mol%, (c) 8mol%, (d) 30mol%

Fig.4 Binding energy of Sn3*d* in $ZnSnO_3$ films with different doping levels of Sb

Table 2 Binding energy of Sn3d and percentages of tin in different chemical states in $ZnSnO_3$ films with different dopings of Sb

Dopingconcentration / mol%	$Sn^{I}3d_{5/2}$		$Sn^{II}3d_{5/2}$		$Sn^{I}3d_{3/2}$		$Sn^{II}3d_{3/2}$	
	Peak / eV	Content / %	Peak / eV	Content / %	Peak / eV	Content / %	Peak / eV	Content / %
0	486.2	100		0	494.6	100		0
1	486.4	66.0	487.0	34.0	494.7	66.0	495.3	34.0
8	486.3	85.0	487.0	15.0	494.7	85.0	495.3	15.0
30	486.0	100		0	494.5	100		0

site.

From the above analysis of Sb3$d_{3/2}$ spectra, Sb^{5+} is the main chemical state when doping level is 1mol%. The process of substituting of Sb ions could be considered as shown in Eq.**1**

$$xSb_2O_5 \rightarrow Zn_{Zn}+2xSb_{Sn}^{\cdot}+xSn_{Sn}^{''}+(1-4x)Sn_{Sn}+3O_O \quad \text{Eq.1}$$

where $Sb_{Sn}^{\cdot}$ is the Sb^{5+} ions replacing the Sn^{4+} sites with one positive charge and $Sn_{Sn}^{''}$ is the Sn^{4+} ions being reduced to Sn^{2+} ions at the same time in order to maintain the electrical neutrality of the crystal. Possible cation vacancies, such as zinc ion vacancy or tin ion vacancy, which is not listed in equation, could also appear to balance electrovalence in the crystal lattice. However, due to similar binding energy of Sn^{2+} and Sn^{4+}, it is hard to separate their Gaussian lines and actual contents of Sn^{4+} and Sn^{2+} in Sb doped $ZnSnO_3$ films are unsure.

If Sn^{4+} ions are assumed to be substituted by Sb^{3+} ions, oxygen vacancy would appear to keep electrovalence balance in the crystal lattice. The process could be considered as shown in Eq.**2**.

$$ySb_2O_3 \rightarrow Zn_{Zn}+2ySb_{Sn}^{'}+yV_O^{\cdot\cdot}+(1-2y)Sn_{Sn}+(3-y)O_O \quad \text{Eq.2}$$

where $Sb_{Sn}^{'}$ is the Sb^{3+} ions replacing the Sn^{4+} sites with one negative charge and $V_O^{\cdot\cdot}$ is the oxygen vacancy formed at the same time in order to maintain the electrical neutrality of the crystal. Due to the existence of Sn ion adjacent to oxygen vacancy gained from XPS analysis, the assumption for the substitution of Sn^{4+} by Sb^{3+} is proved to be true. According to Table 1, the contents of Sb^{3+} increase with the

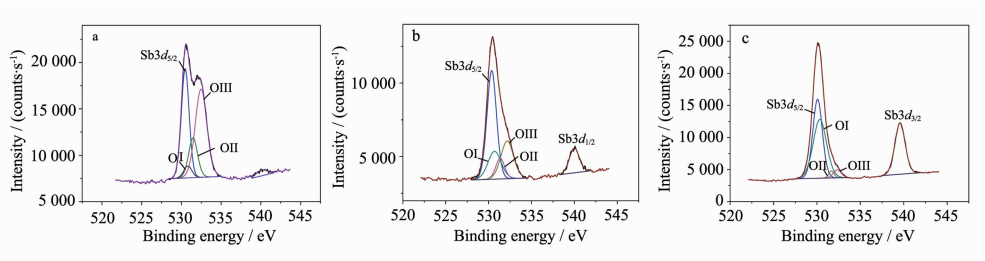

(a) 1mol%, (b) 8mol%, (c) 30mol%

Fig.5　Binding energy of O1*s* in $ZnSnO_3$ films with different doping levels of Sb

increase of antimony ion doping. So oxygen vacancy might increase accordingly (Eq.**2**.).

However, the contents of tin adjacent to oxygen vacancy in 1mol%, 8mol% and 30mol% Sb doped $ZnSnO_3$ films are 34.0%, 15.0%, 0%. The oxygen vacancy is on decline even though increasing Sb substitution. Therefore, it is predicted that defects other than oxygen vacancy might occur along with substitution of Sn^{4+} by Sb^{3+} in $ZnSnO_3$ crystal lattice.

O1*s* spectra of $ZnSnO_3$ films with 1mol%, 8mol% and 30mol% of antimony ion doping are shown in Fig.5 (a) ~(c). The binding energies centered at (530.45±0.3) eV (O Ⅰ), (531.4±0.3) eV (O Ⅱ) and (532.4±0.3) eV (O Ⅲ) suggest the existence of three different environments of oxygen. The peak at (530.45 ±0.3) eV is attributed to oxygen in crystal lattice. The peak at (531.4±0.3) eV is due to O^{2-} ions in an oxygen deficient region and the peak at (532.4± 0.3) eV is assigned to oxygen of free hydroxyl groups which is possibly due to environmental moisture trapped in the surfaces of films[12]. The O1*s* peak of SnO_2 and/or SnO and Sb3$d_{5/2}$ peak are very close, making the division of the individual contribution difficult. So parameters used for division of all spectra include the intensity ratio of Sb3$d_{5/2}$/Sb3$d_{3/2}$=1.5. The spin orbit splitting of the Sb3*d* line is 9.3 eV. The results are shown in Table 3. The contents of oxygen vacancy in $ZnSnO_3$ films with 1mol%, 8mol% and 30mol% of Sb are 29.8%, 15.1% and 4.8%, whose variation tendency is consistent with the results obtained from Sn3*d* peak fitting of Sn ions adjacent to oxygen vacancy.

In addition, the peak area of O1*s* at about 532.4 eV in water molecules absorbed on $ZnSnO_3$ films reduces gradually. As shown in Fig.5 (a) ~(c). The trends are consistent with the decreasing voids present on the film surfaces shown in SEM photographs (Fig.2). In general, water could be absorbed by the voids in a material, resulting in the enhancement of peak area of O1*s* in water molecules.

Zn2*p* spectra of $ZnSnO_3$ films without doping Sb and with 1mol%, 8mol% and 30mol% of Sb are shown in Fig.6(a)~(d). The Zn2$p_{3/2}$ spectra and Zn2$p_{1/2}$ spectra could be respectively separated into two Gaussian lines. The binding energy of Zn2$p_{3/2}$ peaks is centered at (1 020.5±0.3) eV (Zn Ⅰ) and (1 021.8±0.3) eV (Zn Ⅱ). The binding energy of Zn2$p_{1/2}$ peaks is centered at (1 043.5±0.3) eV(Zn Ⅰ) and (1 044.8±0.3) eV (Zn Ⅱ). Zn Ⅰ and Zn Ⅱ represent interstitial zinc ions and lattice zinc ions, respectively[12]. The fitted results are shown in Table 4. The contents of interstitial zinc ions in $ZnSnO_3$ films with 1mol%, 8mol% and

Table 3　Binding energy of O1s and percentages of oxygen in different chemical states in $ZnSnO_3$ films with different doping levels of Sb

Doping concentration /	$O^{Ⅰ}1s$		$O^{Ⅱ}1s$	
mol%	Peak / eV	Content / %	Peak / eV	Content / %
1	530.5	70.2	531.5	29.8
8	530.4	84.9	531.4	15.1
30	530.1	95.2	531.7	4.8

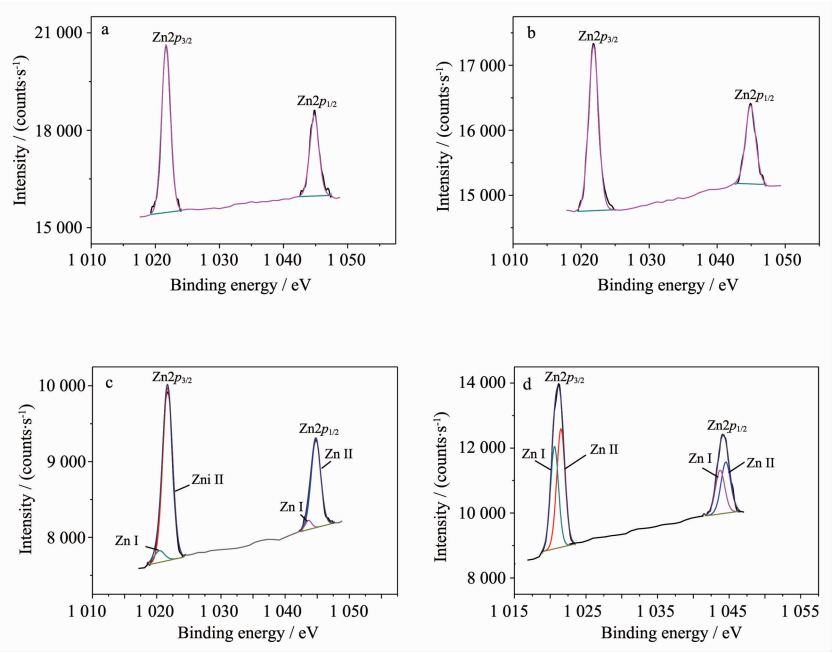

(a) 0mol%, (b) 1mol%, (c) 8mol%, (d) 30mol%

Fig.6 Binding energy of Zn2$p_{3/2}$ and Zn2$p_{1/2}$ in $ZnSnO_3$ films with different doping levels of Sb

Table 4 Binding energy of Zn2*p* and percentages of zinc in different chemical states in $ZnSnO_3$ films with different doping levels of Sb

Doping concentration / mol%	$Zn^{Ⅰ}2p_{3/2}$		$Zn^{Ⅱ}2p_{3/2}$		$Zn^{Ⅰ}2p_{1/2}$		$Zn^{Ⅱ}2p_{1/2}$	
	Peak / eV	Content / %	Peak / eV	Content / %	Peak / eV	Content / %	Peak / eV	Content / %
0		0	1 021.7	100		0	1 044.8	100
1		0	1 021.8	100		0	1 044.9	100
8	1 020.4	6.7	1 021.7	93.3	1 043.6	6.7	1 044.8	93.3
30	1 020.6	45.4	1 021.5	54.6	1 043.8	45.4	1 044.5	54.6

30mol% of Sb are respectively 0%, 6.7%, 45.4%. These interstitial zinc ions are probably formed by substitution of Sn^{4+} by Sb^{3+} to keep the lattice charge in balance. The process can be considered as shown in Eq.**3**

$$zSb_2O_3 \rightarrow Zn_{Zn}+2zSb_{Sn}+zZn_i^{\cdot\cdot}+(1-2z)Sn_{Sn}+3O_O \quad \text{Eq.3}$$

where $Sb_{Sn}^{'}$ is the Sb^{3+} ions replacing the Sn^{4+} sites with one negative charge and $Zn_i^{\cdot\cdot}$ is the interstitial zinc ion formed at the same time in order to maintain the electrical neutrality of the crystal. The contents of interstitial ions increase with the increase of Sb1 doping as well as contents of Sb^{3+} ions. From XPS analysis of oxygen and zinc, defects as oxygen vacancy and interstitial zinc ion are found to balance the negative charge formed by substitution of Sn^{4+} by Sb^{3+} in Sb doped $ZnSnO_3$ films. When Sb^{3+} ions are few, oxygen vacancy dominates. When Sb^{3+} ions increase, oxygen vacancy decreases while interstitial zinc ion increases until finally interstitial zinc ions become the principle defect. However, original $ZnSnO_3$ crystal lattice would be unstable unless Zn ions in crystal lattice are replaced by parts of Sb ions, making large amounts of Zn ions enter into the interstitial sites of crystal lattice. Anyway this substitution is possible from the perspective of ionic radii.

From all XPS analysis, Sb ions detected in $ZnSnO_3$ films are in two oxidation states as pentavalent state (Sb^{5+}) and tervalent state (Sb^{3+}). With increasing doping of Sb, the contents of Sb^{5+} ions decrease while that of Sb^{3+} ions increase, leading to

more substitution of Sn^{4+} by Sb^{3+}. Meanwhile, oxygen vacancies and interstitial zinc ions appear to maintain electrical neutrality in the crystal lattice. However, with increasing antimony ion doping, the contents of oxygen vacancies decrease while that of interstitial zinc ions increase.

2.3 Electrical properties of $ZnSnO_3$ films

To clarify the influence of antimony ion doping on resistivity, carrier concentration and mobility, the Hall measurement was used to examine these electrical properties of $ZnSnO_3$ films with 0mol%, 1mol%, 8mol% and 30mol% of Sb. Results are listed in Table 5. The carrier concentration and mobility of undoped $ZnSnO_3$ films are 8.5×10^{16} cm^{-3} and 1.440 $cm\cdot V^{-1}\cdot s)^{-1}$, resulting in resistivity of 51.0 Ω·cm. For $ZnSnO_3$ films with antimony ion doping from 1mol% to 8mol%, the mobility values are similar. The carrier concentrations increase from 3.9×10^{18} cm^{-3} to 5.5×10^{18} cm^{-3}, resulting in the minimum resistivity of 0.96 Ωcm in films with 8mol% of antimony ion doping. For $ZnSnO_3$ films with 30mol% of Sb, the carrier concentration increases to 1.5×10^{19} cm^{-3} while the mobility decreases remarkably, thus leading to a higher resistivity of 5.90 Ω·cm. The variation trends of carrier concentration, mobility and resistivity are shown in Fig.7.

Table 5　Resistivity, carrier concentration and mobility of $ZnSnO_3$ films with different doping levels of Sb

Doping Concentration / mol%	Resistivity / (Ω·cm)	Concentration / cm^{-3}	Mobility / $(cm\cdot V^{-1}\cdot s^{-1})$
0	51.0	8.5×10^{16}	1.440
1	1.30	3.9×10^{18}	1.100
8	0.96	5.5×10^{18}	1.150
30	5.90	1.5×10^{19}	0.068

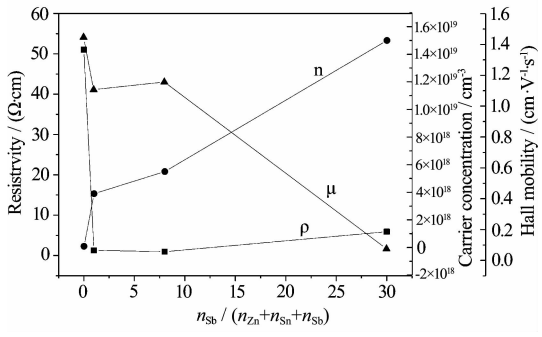

Fig.7　Resistivity, carrier concentration and mobility of $ZnSnO_3$ films with different doping levels of Sb

According to Hall measurements, $ZnSnO_3$ films are n-type semiconductors, whose majority carriers are electrons. Meanwhile, the carrier concentration increases significantly from 8.5×10^{16} cm^{-3} to 1.5×10^{19} cm^{-3}. For XPS analysis, two defects offering electrons as oxygen vacancy and interstitial zinc ion exist in Sb doped $ZnSnO_3$ films. With the increase of antimony ion doping, the contents of oxygen vacancies decrease while that of interstitial zinc ions increase. Only the variation trend of interstitial zinc ions is consistent with that of carrier concentration. Therefore, interstitial zinc ions can be considered as the main free carrier for $ZnSnO_3$ films. The result matches well with our previous report of conductive mechanism of $ZnSnO_3$ thin films [23]. However, with the increase of interstitial zinc ions as well as carrier concentrations, the resistivity of $ZnSnO_3$ films does not always decrease and a minimum resistivity is obtained at 8% molar ratio of Sb. Therefore, the high antimony ion concentration, which leads to a lower carrier mobility, is one of the crucial factors limiting the electrical properties. Our future work is to find a more suitable dopant which can provide higher concentration of interstitial zinc ions at low ion doping concentrations, thus achieving $ZnSnO_3$ thin films with both high carrier concentration and mobility.

2.4 UV-Vis light transmissions

The optical-transmission spectra of $ZnSnO_3$ films with different doping levels of Sb are shown in Fig.8 (a)~(c). The average transmittances of $ZnSnO_3$ films with 1mol% and 8mol% of Sb in visible region are all above 80%. The minimum transmittance of $ZnSnO_3$ films with 30mol% of Sb is 65% in visible region of

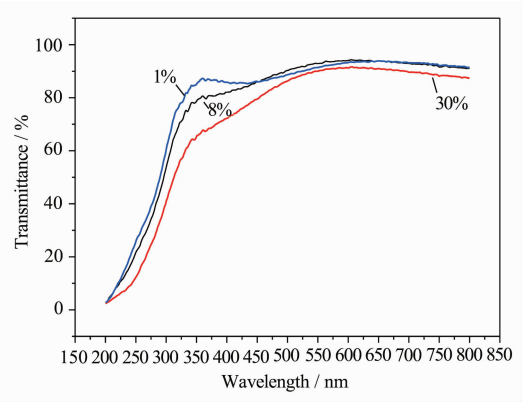

Fig.8 UV-Vis light transmission of $ZnSnO_3$ films with different doping levels of Sb

475 nm to 380 nm while in region larger than 475 nm, the transmission is above 80%. The scattering centers and crystal boundaries aroused by antimony ion doping account for this decrease.

3.3 Conclusions

In this study, $ZnSnO_3$ films with different doping levels of Sb were prepared by sol-gel spin-coating method. With increasing doping of Sb, the contents of Sb^{3+} ions increase and that of Sb^{5+} ions decrease in $ZnSnO_3$ solid solution. Meanwhile, interstitial zinc ions increase and oxygen vacancies decrease. $ZnSnO_3$ films are n-type semiconductors. The carrier concentrations increase with the increase of free electrons offered by interstitial zinc ions in $ZnSnO_3$ lattice. However, due to the decreasing carrier mobility, the minimum resistivity (0.96 Ω·cm) is obtained with 8 mol% of antimony ion doping. The average transmissions of all films prepared are over 80% in region larger than 475 nm.

Acknowledgments: The authors gratefully acknowledge the financial support from the National Natural Science Foundation of China.

References:

[1] Fortunato E, Ginley D, Hosono H, et al. *MRS Bull.*, **2007**, **32**:242-247

[2] Porch A, Morgan D V, Perks R M, et al. *J. Appl. Phys.*, **2004**, **95**:4734-4737

[3] Marks T J, Veinot J G C, Cui J, et al. *Synth. Met.*, **2002**, **127**:29-35

[4] Ginley D S, Bright C. *MRS Bull.*, **2000**,**25**:15-18

[5] Popovi J, Greta B, Tkalec E. *Mater. Sci. Eng., B*, **2011**,**176**: 93-98

[6] Fan J C C, Goodenough J B. *J. Appl. Phys.*, **1997**,**48**:3524-3531

[7] Moholkar A V, Pawar S M, Rajpure K Y, et al. *Appl. Surf. Sci.*, **2009**,**255**:9358-9364

[8] Nasr B, Dasgupta S, Wang D. *J. Appl. Phys.*, **2010**,**108**: 103721-1-103721-6

[9] Coutts T J, Young D L. *J. Vac. Sci. Technol. A*, **2000**,**18**(6): 2646-2660

[10]Jain V K, Kumar P, Bhandari D. *Thin Solid Films*, **2010**, **519**:1082-1086

[11]Lee Y E, Norton D P, Budai J D. *J. Appl. Phys.*, **2001**,**90**: 3863-3866

[12]Jain V K, Kumar P, Kumar M. *J. Alloys Compd.*, **2011**,**509**: 3541-3546

[13]Hayashi Y, Kondo K, Murai K, et al. *Vacuum*, **2004**,**74**:607-611

[14]Kurz A, Aegerter M A. *Thin Solid Films*, **2008**,**516**:4513-4518

[15]Kurz A, Brakecha K, Puetz J. *Thin Solid Films*, **2006**,**502**: 212-218

[16]Ko J H, Kim I H, Kim D. *Appl. Surf. Sci.*, **2007**,**253**:7398-7403

[17]Knapp C E, Hyett G, Parkin I P. *Chem. Mater.*, **2011**,**23**: 1719-1726

[18]Tetsuka H, Shan Y J, Tezuka K. *Vacuum*, **2006**,**80**:1038-1041

[19]Inoue K, Tominaga K, Tsuduki T. *Vacuum*, **2009**,**83**:552-556

[20]Minami T, Tsukada S, Minamino Y. *J. Vac. Sci. Technol. A*, **2005**,**23**(4):1128-1132

[21]Minami T. *MRS Bull.*, **2000**,**25**:38-44

[22]Minami T, Miyata T, Yamamoto T. *Surf. Coat. Technol.*, **1998**,108-109:583-587

[23]Mianami T, Sonohara H, Sato H, et al. *Jpn. J. Appl. Phys.*, **1994**,**33**:1693-1696

[24]Inaguma Y, Yoshida M, Katsumata T. *J. Am. Chem. Soc.*, **2008**,**130**:6704-6705

[25]Xue X Y, Chen Y J, Wang Y G, et al. *Appl. Phys. Lett.*, **2005**,**86**:233101(1-3)

[26]JI Ling-Li(季伶俐), HE Yun-Qiu(贺蕴秋), LI Le(李乐). *Chinese J. Inorg. Chem.*(无机化学学报), **2012**,**28**(3):437-444

[27]Hoel C A, Mason T O, Gaillard J F. *Chem. Mater.*, **2010**,**22**: 3569-3579

[28]Laurent A, Josette O F. *J. Power Sources*, **2003**,**119-121**: 585-590